JBC RESEARCH ARTICLE

Interaction between the transmembrane domains of neurotrophin receptors p75 and TrkA mediates their reciprocal activation

Received for publication, May 21, 2021, and in revised form, June 25, 2021 Published, Papers in Press, July 1, 2021,
https://doi.org/10.1016/j.jbc.2021.100926

María L. Franco[1,‡], Kirill D. Nadezhdin[2,‡], Taylor P. Light[3], Sergey A. Goncharuk[2,4], Andrea Soler-Lopez[1], Fozia Ahmed[3], Konstantin S. Mineev[2,4], Kalina Hristova[3], Alexander S. Arseniev[2,*], and Marçal Vilar[1,*]

From the [1]Unit of Molecular Basis of Neurodegeneration, Institute of Biomedicine CSIC, València, Spain; [2]Department of Structural Biology, Laboratory of NMR-Spectroscopy, Shemyakin-Ovchinnikov Institute of Bioorganic Chemistry of the Russian Academy of Sciences, Moscow, Russian Federation; [3]Department of Materials Science and Engineering, Johns Hopkins University, Baltimore, Maryland, USA; and [4]Phystech School of Biological and Medical Physics, Moscow Institute of Physics and Technology, Moscow, Russian Federation

Edited by Wolfgang Peti

The neurotrophin receptors p75 and tyrosine protein kinase receptor A (TrkA) play important roles in the development and survival of the nervous system. Biochemical data suggest that p75 and TrkA reciprocally regulate the activities of each other. For instance, p75 is able to regulate the response of TrkA to lower concentrations of nerve growth factor (NGF), and TrkA promotes shedding of the extracellular domain of p75 by α-secretases in a ligand-dependent manner. The current model suggests that p75 and TrkA are regulated by means of a direct physical interaction; however, the nature of such interaction has been elusive thus far. Here, using NMR in micelles, multiscale molecular dynamics, FRET, and functional studies, we identified and characterized the direct interaction between TrkA and p75 through their respective transmembrane domains (TMDs). Molecular dynamics of p75-TMD mutants suggests that although the interaction between TrkA and p75 TMDs is maintained upon mutation, a specific protein interface is required to facilitate TrkA active homodimerization in the presence of NGF. The same mutations in the TMD protein interface of p75 reduced the activation of TrkA by NGF as well as reducing cell differentiation. In summary, we provide a structural model of the p75–TrkA receptor complex necessary for neuronal development stabilized by TMD interactions.

Nerve growth factor (NGF) is a member of the mammalian neurotrophin (NT) protein family, which also includes brain-derived neurotrophic factor, NT3, and NT4/5 (1). NTs are implicated in the maintenance and survival of the peripheral and central nervous systems and mediate several forms of synaptic plasticity (2–5). NTs interact with two distinct receptors, a cognate member of the tyrosine protein kinase receptor A (TrkA) family and the common p75 NT receptor, which belongs to the tumor necrosis factor receptor (TNFR) superfamily of death receptors (6, 7). Trk receptor signaling is involved in survival and differentiation (8, 9), whereas p75 participates in several signaling pathways (reviewed in Ref. (10)). p75-mediated signaling is governed by the cell context and the formation of complexes with different coreceptors and ligands, such as sortilin/pro-NGF in cell death (11), Nogo/Lingo-1/NgR in axonal growth (12, 13), and TrkA/NGF in survival and differentiation (14). p75 also undergoes shedding and receptor intramembrane proteolysis, resulting in the release of its intracellular domain (ICD), which itself possesses signaling capabilities (15–17).

Several lines of evidence implicate functional interactions between TrkA and p75NTR in NGF-triggered signal transduction (3, 18–20). TrkA and p75 receptors have nanomolar affinities for NGF and cooperate in transducing NGF signals (7, 21). The expression patterns of these two receptors overlap extensively (22), and in some instances, such as in the neurons of the dorsal root ganglion, TrkA is exclusively expressed in conjunction with p75 (23).

p75 has been experimentally demonstrated to enhance the response of TrkA to NGF (14, 24–26). In sympathetic neurons and oligodendrocytes, TrkA signaling inhibits the pro-apoptotic signaling of p75 (27–29). Primary dorsal root ganglion and sympathetic neurons derived from p75-null animals show attenuated survival responses to NGF (25, 26, 30), confirming the physiological role of p75–TrkA interactions. As the interaction between the two receptors seems to not engage the ligand-binding domains of the extracellular region (31), the structural basis of such direct interaction is still unknown.

Here, we demonstrate that the interaction between TrkA and p75 is mediated, at least in part, by the transmembrane domains (TMDs). We validate these findings using functional studies in cells expressing the full-length receptors.

‡ These authors contributed equally to this work.
* For correspondence: Marçal Vilar, mvilar@ibv.csic.es; Alexander S. Arseniev, aars@nmr.ru.

Results

p75 and TrkA form a constitutive complex at the plasma membrane

We performed FRET experiments to determine if TrkA and p75 interact directly at the plasma membrane of live cells. Human embryonic kidney 293T (HEK 293T) cells transiently cotransfected with full-length TrkA tagged with mTurquoise (mTurq; the donor fluorescent protein) and full-length p75 tagged with enhanced YFP (eYFP) (the acceptor fluorescent protein) were imaged, and small regions of the plasma membrane were selected and analyzed. Illustrations of the TrkA-mTurq and p75-eYFP constructs used in FRET experiments are shown in Figure 1*A*. In each region of the cell membrane, we determined the FRET efficiency, the concentration of TrkA-mTurq, and the concentration of p75-eYFP using the fully quantified spectral imaging (FSI)–FRET software (Fig. 1*B*) (32). These experiments were designed such that FRET can only occur between TrkA and p75, not between TrkA–TrkA and p75–p75. We also performed control FSI–FRET experiments using two unrelated proteins, linker for the activation of T-cells (LAT) and fibroblast growth factor receptor 3 (FGFR3), which are not expected to interact specifically and thus should give zero hetero-FRET. In addition, the proteins were designed such that the fluorescent tags are positioned differently with respect to the plasma membrane—the mTurq fluorophore is attached to the C terminus of full-length LAT, whereas the eYFP fluorophore is attached to the C terminus of an FGFR3 construct lacking the intracellular region, "ECTM" (Fig. 1*A*). Therefore, these two proteins will also not give rise to a nonspecific FRET signal (random or "proximity" FRET) (33). As expected, because of the large separation between the fluorescent tags, the FRET efficiencies measured between these two control proteins are localized around zero at all concentrations measured (Fig. 1*B*). Therefore, this control dataset demonstrates the scenario where there is no FRET between the proteins.

In the absence of ligand, full-length TrkA and p75 exhibit positive (greater than zero) FRET efficiency values over all TrkA and p75 concentrations measured (Fig. 1*B*). Therefore, these data suggest that TrkA and p75 interact directly at the plasma membrane. With these data alone, we cannot

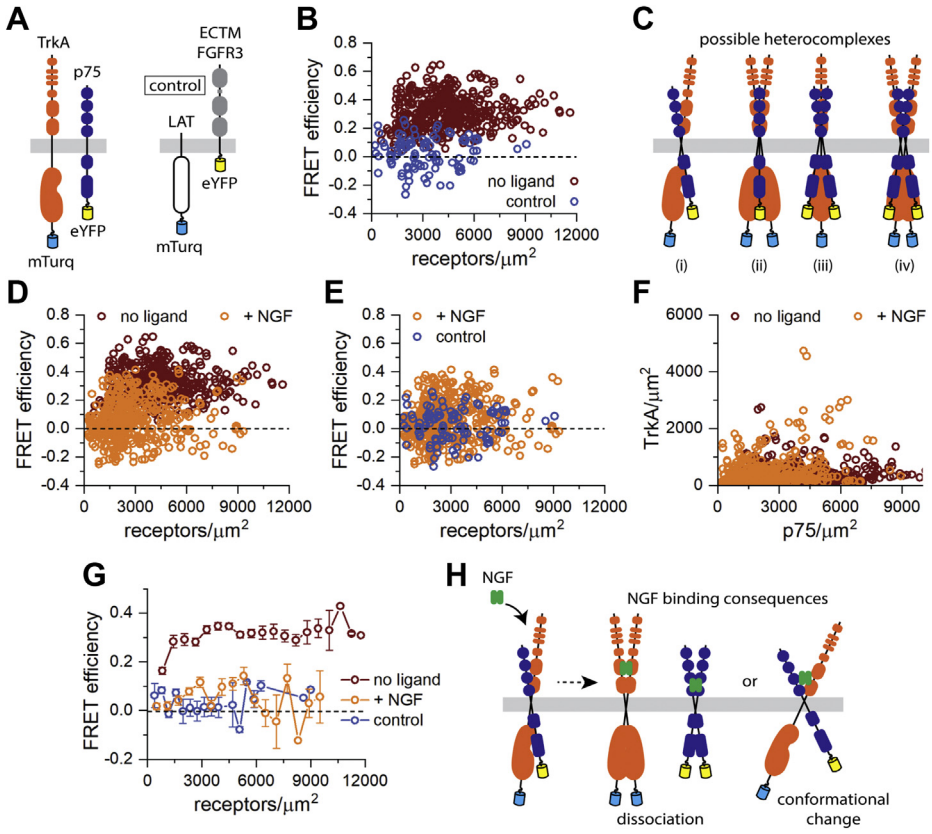

Figure 1. TrkA–p75 FSI–FRET experiments. *A*, illustrations of the TrkA-mTurq and p75-eYFP proteins used in FRET experiments along with the LAT-mTurq and ECTM FGFR3–eYFP proteins used in control experiments. *B*, FRET efficiencies as a function of total receptor concentration measured for TrkA-mTurq and p75-eYFP in the absence of ligand compared with a zero FRET control dataset. *C*, illustrations of some possible stoichiometries of the TrkA–p75 heterocomplex: (i) heterodimer, (ii) heterotrimer of two TrkA and one p75, (iii) heterotrimer of one TrkA and two p75, and (iv) heterotetramer or two TrkA and two p75. *D*, FRET data for TrkA-mTurq and p75-eYFP in the presence of 100 ng/μl NGF compared with the data in the absence of NGF. *E*, the FRET data for TrkA and p75 in the presence of NGF compared with the zero FRET control dataset. *F*, expression of TrkA-mTurq and p75-eYFP measured on the cell surface for the experiments performed in the absence and presence of NGF. *G*, the FRET data for TrkA–p75 in the absence and presence of NGF and for the control dataset were binned and compared. *H*, illustrations of the possible consequences of NGF binding to the TrkA–p75 heterocomplex, which could be either dissociation of the heterocomplex to stabilize the respective homodimers or an NGF-induced conformational change. The bars represent the standard error of the mean. eYFP, enhanced YFP; FGFR3, fibroblast growth factor receptor 3; FSI, fully quantified spectral imaging; LAT, linker for the activation of T-cells; mTurq, mTurquoise; NGF, nerve growth factor; TrkA, tyrosine protein kinase receptor A.

determine an accurate stoichiometry of the TrkA–p75 heterocomplex. Given that TrkA and p75 exist in monomer–dimer equilibrium in the absence of ligand, it is possible that TrkA and p75 associate as heterodimers or oligomers of higher order (Fig. 1*C*). Next, we sought to determine if NGF ligand binding influences the TrkA–p75 heterocomplex, and we performed similar FSI–FRET experiments for TrkA–p75 in the presence of 100 ng/μl NGF (Fig. 1*D*). The FRET efficiencies measured for TrkA–p75 in the presence of NGF are noticeably lower compared with the data in the absence of ligand. Furthermore, comparison of the liganded TrkA–p75 FRET data to the LAT–FGFR3 control experiment data revealed no significant differences (Fig. 1*E*), which suggests that the fluorophores attached to the C termini of TrkA and p75 are too far away from one another to observe a FRET signal in the ligand-bound state. The expression levels of the TrkA and p75 at the cell surface are similar in both sets of experiments (with/without NGF) so these differences are not a reflection of altered gene expression (Fig. 1*F*). The decrease in FRET may mean that the heterointeractions are abolished, for instance, because of ligand-induced homodimer stabilization, or it may be because of conformational changes in the heterocomplex, which leads to decreased FRET.

The FRET data for TrkA–p75 in the absence and presence of NGF and the control dataset were binned and compared in order to visualize the average FRET efficiency as a function of receptor concentration (Fig. 1*G*). For the control dataset and the TrkA–p75 data in the presence of NGF, the average FRET efficiencies remain around zero as expected from the raw data (Fig. 1*G*). For the TrkA–p75 data in the absence of ligand, we observe average FRET efficiencies greater than zero over all concentrations (Fig. 1*G*). Furthermore, at the low receptor concentration regime, the average FRET efficiencies increase as a function of receptor concentration, suggesting increasing TrkA–p75 interactions (Fig. 1*G*).

Direct interaction between p75 and TrkA TMDs

Previous findings have suggested that TrkA can form a complex with p75-CTF (a membrane-anchored C-terminal fragment) by means of TMD interaction (17). In addition, the TMD of p75 is involved in the formation of the high-affinity NGF-binding sites (34), suggesting that the TMD may

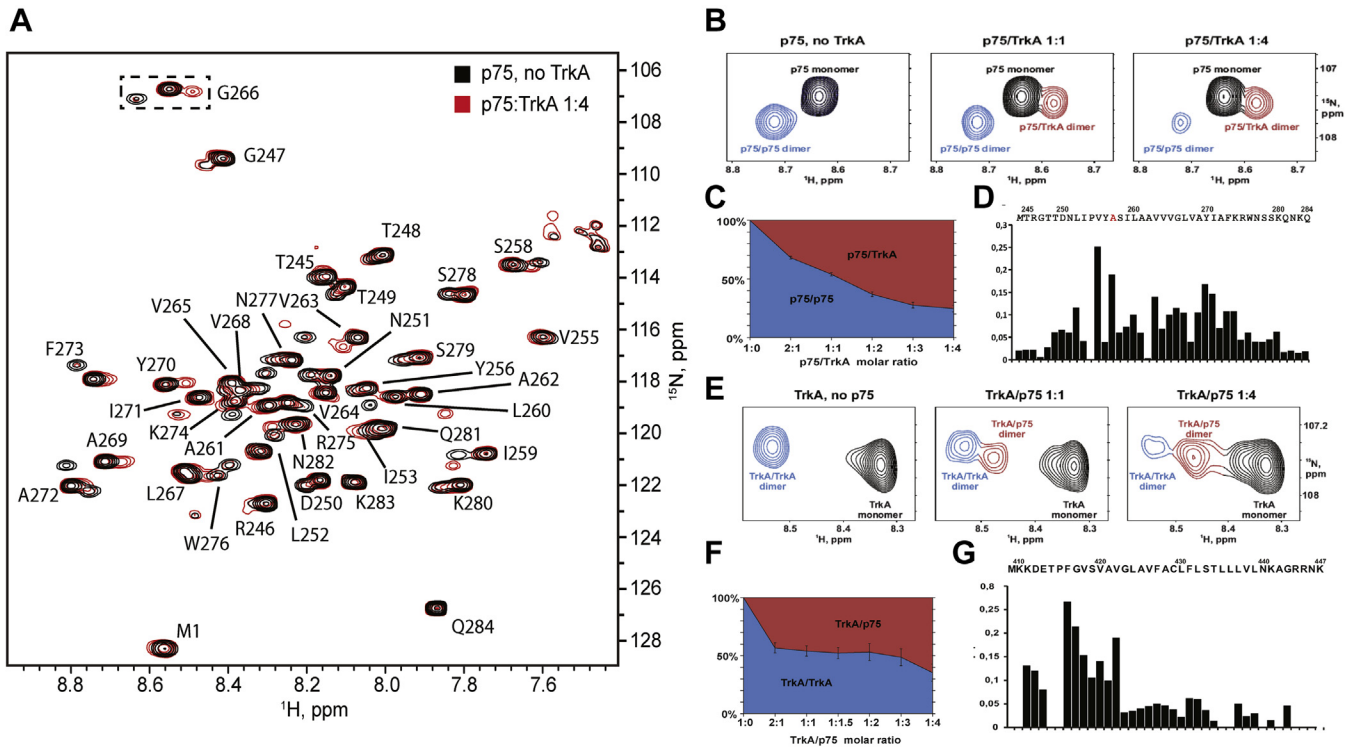

Figure 2. p75–TrkA interactions as observed by NMR. *A*, overlay of two ^{15}N-transverse relaxation optimized spectroscopy experiments: (*black*) ^{15}N-labeled p75 without TrkA and (*red*) ^{15}N-labeled p75 after addition of unlabeled TrkA with p75:TrkA molar ratio of 1:4. ^{1}H–^{15}N assignments of p75 backbone amid proton resonances are provided. *B*, ^{15}N-labeled p75-TM-C257A titration with unlabeled TrkA TM. *Left* to *right*, p75 monomer (*black*), p75-p75 homodimer (*blue*), and p75-TrkA heterodimer (*red*) states are observed in the G266 amide proton crosspeak in ^{1}H/^{15}N-heteronuclear single quantum coherence spectra. G266 was chosen as representative as its crosspeak is situated away from other peaks, and it shows clear monomer–homodimer–heterodimer transitions. *C*, population of p75–p75 homodimers relative to that of p75–TrkA heterodimers (p75–p75 peak intensity is divided by sum of p75–p75 and p75–TrkA peak intensities), expressed as a function of the p75–TrkA molar ratio. The population of p75–p75 dimer decreases, whereas that of p75–TrkA dimer increases as more TrkA is added to the sample. *D*, chemical shift changes observed upon interaction with TrkA are shown on top of p75-TM sequence. *E*, ^{15}N-labeled TrkA-TMD titration with unlabeled p75-TM-C257A. *Left* to *right*, TrkA monomer (*black*), TrkA–TrkA homodimer (*blue*), and p75–TrkA heterodimer (*red*) states are observed in the amide proton crosspeak in ^{1}H/^{15}N-heteronuclear single quantum coherence spectra. *F*, population of TrkA–TrkA homodimers relative to that of TrkA–p75 heterodimers (TrkA–TrkA peak intensity is divided by sum of TrkA–TrkA and TrkA–p75 peak intensities), expressed as a function of the TrkA–p75 molar ratio. The population of TrkA–TrkA dimer decreases, whereas that of TrkA–p75 dimer increases as more p75 is added to the sample. *G*, chemical shift changes observed upon interaction with p75 are shown on top of TrkA-TMD sequence. For all experiments, the lipid-to-protein molar ratio (LPR) remains constant at 80. TM, transmembrane; TMD, transmembrane domain; TrkA, tyrosine protein kinase receptor A.

mediate the direct interaction between p75 and TrkA. Therefore, we were interested in investigating the interaction between the p75 and TrkA, taking into account the recently reported NMR structures of p75 and TrkA TMDs (35, 36). We examined the interaction of p75-TM-wt with the TrkA-TMD in lipid micelles using NMR spectroscopy. Increasing amounts of TrkA-TM were added to the ^{15}N-labeled p75-TM in dodecylphosphocholine (DPC) micelles, and the chemical shifts (CSs) were monitored in a ^{1}H–^{15}N heteronuclear single quantum coherence spectrum (Fig. 2*A*). CSs are very sensitive to the electronic environment of a nucleus and serve as an ideal instrument to probe the protein–protein interaction. Previous work in our laboratory found that p75-TM-wt forms spontaneous disulfide dimers (35). We titrated the ^{15}N-labeled p75-TM-wt disulfide dimer with increasing concentrations of TrkA-TM-wt solubilized in DPC micelles, retaining the constant lipid-to-protein ratio (LPR). The titration revealed no CS changes. We used several LPRs and at least two independent preparations of p75-TM-wt. As the dimerization of p75-TMD-wt is irreversible (35), we performed the experiments with the mutant p75-C257A, which forms noncovalent homodimers (35) and allows the possibility to obtain the monomeric p75-TMD. According to the previous work (35), the C257A mutation does not induce any substantial changes to the structure of p75 TMD. Several CS changes were observed in the heteronuclear single quantum coherence-NMR spectrum of p75-TM-C257A upon titration with TrkA-TM-wt, suggesting the formation of specific p75–TrkA heterocomplexes (Fig. 2*B*).

To identify the oligomer size of the complex, we measured the cross-correlated relaxation rates of p75-TM-C257A signals (Fig. S1). According to the recent work, the NMR-derived hydrodynamic radii of TMDs in DPC micelles can be used to distinguish the various oligomeric forms of the proteins (37). Here, we observed the rotational correlation time (and hydrodynamic radius) of a p75-TM-C257A monomer at 45 °C to be 10.2 ± 0.4 ns (2.61 nm), a p75-TM-C257A homodimer to be 13.1 ± 0.6 ns (2.85 nm), and the heterocomplex to be 12.7 ± 0.8 ns (2.82 nm). In other words, the observed new complex formed by TrkA-TM and p75-TM-C257A is a heterodimer as the rotational correlation time of the heterocomplex was similar to that of the homodimer.

With the increase of TrkA concentration, the percentage of p75 homodimer decreased, whereas that of p75–TrkA heterodimer increased (Fig. 2*C*). This implies that homodimerization and heterodimerization of p75-TM are the competing processes. The titration curve revealed homodimerization and heterodimerization constants of comparable magnitudes. Similar effects were observed when ^{15}N-labeled TrkA-TMD sample was titrated with the unlabeled p75-TM-C257A (Fig. 2, *E* and *F*). Addition of p75-TM-C257A decreased the concentration of TrkA-TM homodimer, whereas the novel heterodimeric state had emerged, which is indicative of the competition. Thus, we can state that TrkA interacts with the monomeric form of p75 TMD but does not bind the disulfide-crosslinked dimer of the protein. Most likely, the covalent dimerization shields some of the p75 residues necessary to interact with the TrkA TMD, or the interaction requires a rearrangement of the dimer that cannot be achieved because of the restraints imposed by the disulfide bonds.

CS changes were detected along the p75 TMD sequence (Fig. 2*D*), which is expected as the TrkA interaction breaks the p75-TM-C257A dimerization. The residues with the highest CS changes are shown in Figure 2*D*. To find the residues undergoing CS changes in the TrkA-TMD, we performed the titration on labeled ^{15}N-TrkA-TMD homodimer with unlabeled p75-TM-C257A (Fig. 2*E*). With increasing p75-TM-C257A concentration, the percentage of TrkA homodimer decreased, whereas the heterodimer increased (Fig. 2*F*). The NMR CSs indicated that the region of higher CS changes (Fig. 2*G*; $\Delta\delta > 0.1$) upon interaction of p75-TMD is located mainly at the N terminus of TrkA TMD.

These results support a direct interaction between p75-TMD and TrkA-TMD and suggest that the formation of a heterodimer outcompetes the homodimerization of each TMD. Although the NMR shows that the interaction is direct, we cannot use the CS changes to identify the protein–protein interface between the TMDs in a membrane. Recently, it has been shown that, by contrast to soluble proteins, CS changes have almost zero predictive power to map protein interfaces in transmembrane regions (38). CS changes primarily report hydrogen bonding and are insensitive to van der Waals contacts between the protein side chains, which are the main driving force for dimerization of membrane proteins (38).

Multiscale molecular dynamics

The crowding of the NMR spectra with several TrkA and p75 species (monomer, homodimer, and heterodimer) precludes the complete CS assignment and the structure calculation of the heterocomplex. To explore further the interaction between TrkA and p75 TMDs, we used molecular dynamics (MD) (Fig. 3). MD simulations provide a useful approach for modeling the TMD interactions (39). Both full-atom (FA) and coarse-grained (CG) modeling has been previously used to optimize the dynamics and interactions between different TMDs (39). To model the heterodimerization of p75-TMD and TrkA-TMD, two CG helices were inserted in a parallel orientation relative to one another separated 6 nm in a preformed 1-palmitoyl-2-oleoyl-sn-glycero-3-phosphocholine (POPC) bilayer, and 24 simulations of 5 μs were run (total time of 120 μs) (Table S1 and Fig. 3*A*). In all but one of the 12 simulations, the TrkA–p75 heterodimer was formed within the first 2 μs (except for the simulation number #5 that formed the heterodimer at 5 μs) and did not dissociate during the remainder of the simulation (Fig. 3*B*). The POPC model membrane was well equilibrated with average values for the area per lipid and hydrophobic thickness (between glycerol groups) of 63.2 Å^2 and 34.8 Å, respectively, that are in good agreement with the experimental values (40) (Table S2). From each of the heterocomplexes (Fig. 3*C*), we compute the RMSD between them and found a cluster of seven models with an average RMSD of 2.12 Å (Fig. 3*D*). The final model was converted from CG to FA to further study the packing of the interaction in a POPC lipid bilayer during 100 ns of FA-MD,

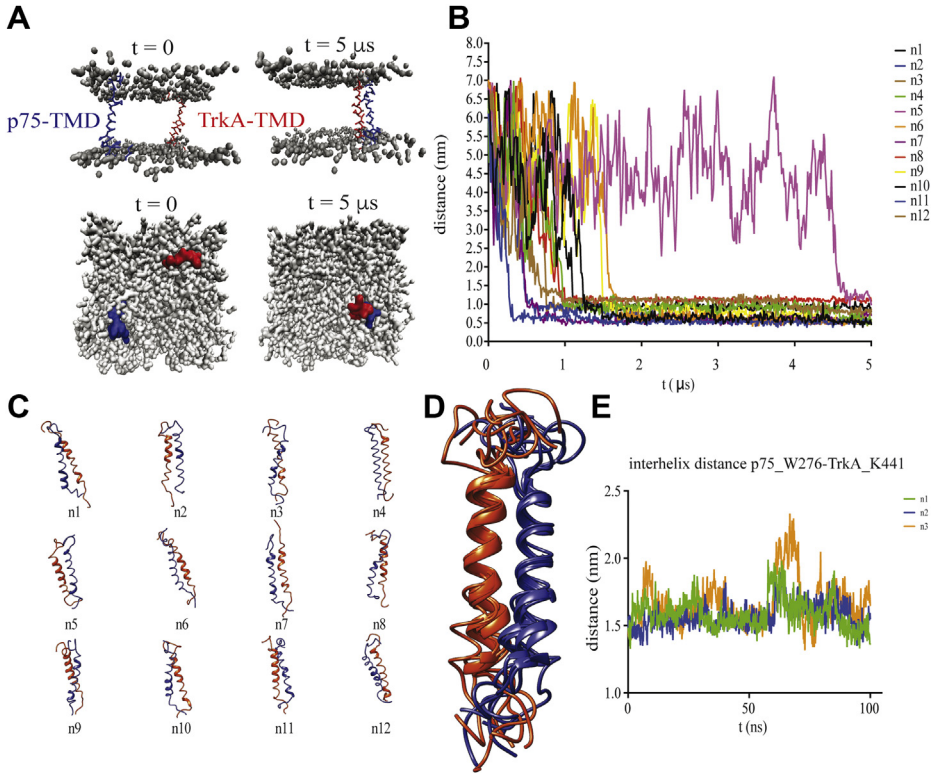

Figure 3. Multiscale MD of TrkA-TMD and p75-TMD. *A*, coarse-grained TrkA-TMD and p75-TMD helix dimerization simulation. The initial system configuration (0 μs) consists of two helices (*red* and *blue*) inserted in a POPC bilayer in a parallel orientation with an interhelix separation of interhelical distance (dHH) ≈ 55 Å. The choline, phosphate, and glycerol (*gray*) backbone particles of the POPC molecules are shown. The snapshot at 5 μs illustrates the stable TM helix heterodimer. *B*, distance between TrkA-TMD and p75-TMD during CG-MD simulation time. *C*, structural models of the final conformations from the 12 simulations. In *blue* p75 and in *red* TrkA is shown. *D*, superposition of the seven conformations with lowest RMSD found by CG-MD. *E*, interhelical distance between p75-TMD-W276 and TrkA-TMD-K441 in the FA-MD simulation done by triplicate. CG, coarse-grained; MD, molecular dynamics; POPC, 1-palmitoyl-2-oleoyl-sn-glycero-3-phosphocholine; TM, transmembrane; TMD, transmembrane domain; TrkA, tyrosine protein kinase receptor A.

done in triplicate. The final POPC model membrane was well equilibrated with average values for the area per lipid and hydrophobic thickness (between phosphate groups) of 63.3 $Å^2$ and 38.4 Å, respectively, which are in good agreement with the experimental values (40). The electron density of the membrane was calculated and shown in Fig. S2. The interhelix distance between residues at the C terminus of the helix (p75-W276 and TrkA-K441) was calculated along the total

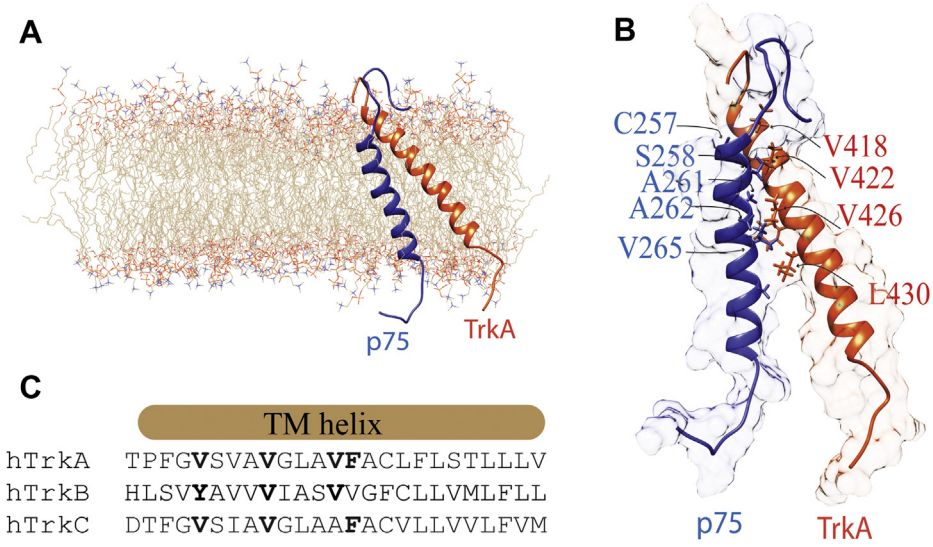

Figure 4. Structural models of the p75–TrkA TMD heterodimer. *A* and *B*, schematic representation of the spatial structure of the heterodimer p75-TMD (*blue*) and TrkA-TMD (*orange*) after 100 ns full-atom MD. The residues participating in the dimer interface are shown in *blue* (p75) and *red* (TrkA). *C*, protein sequence alignment of TrkA, TrkB, and TrkC TMDs. In *bold* are the conserved residues. MD, molecular dynamics; TMD, transmembrane domain; TrkA, tyrosine protein kinase receptor A.

simulation time (Fig. 3*E*), indicating the equilibration of a stable complex.

The protein interface of p75-TMD participating in the interaction with TrkA-TMD is $C_{257}S_{258}xxA_{261}A_{262}xxV_{265}G_{266}xxA_{269}xx$ (Fig. 4, *A* and *B*). This interface contains the motif $A_{262}xxxG_{266}xxA_{269}$ that was previously identified in the homodimerization of p75-TMD-C257A (35) and is supported by the NMR experiments shown previously, indicating that heterodimerization with TrkA-TMD competes with the p75-TMD noncovalent homodimerization. In addition, the C257 residue forms a part of the heterodimer interface supporting our observations that disulfide dimers do not significantly bind to the TrkA-TMD. The TrkA-TMD heterodimer interface is formed by the motif $V_{418}xxxV_{422}xxxV_{426}F_{427}xxL_{430}$ (Fig. 4*B*) where the central valine residues make the closest contact with the p75-TMD. Interestingly, several of these residues are conserved in TrkB and TrkC (Fig. 4*C*) suggesting that these receptors interact with p75 in a similar manner as TrkA.

Altogether, the NMR and FRET data support the direct interaction between TrkA and p75, and the MD provides insight into a possible heterodimer model.

The transmembrane heterodimer interface modulates TrkA activation and sensitization to lower concentrations of NGF

In vivo data suggest that in sensory neurons, p75 helps TrkA to respond to the lower concentrations of NGF (26) and enhances the response of TrkA to NGF (14, 24). One current hypothesis is that the binding of p75 to TrkA induces a conformational change in TrkA that facilitates both the binding of NGF to TrkA (24) and the activation of TrkA (26). To test if the protein interface found previously has any physiological role, we sought to determine if mutations on the p75 transmembrane protein interface influences TrkA activation to lower concentrations of NGF (Fig. 5*A*). We coexpressed p75 with TrkA full-length receptors in HeLa cells and stimulated with increasing concentrations of NGF (0, 0.1, 1, 10, and 100 ng/ml). Western blot analysis of cell lysates was probed with specific antibodies against the activation loop of the TrkA kinase domain (Tyr675 and Tyr676) (Fig. 5*B*). Quantification of the protein bands corresponding to the phosphorylation of TrkA was plotted against NGF concentration. Fitting the data to a dose (NGF)–response (phosphorylation) curve allows an estimation of the EC_{50} of NGF, the concentration of NGF that provokes a response halfway between the basal response and the maximal response (Fig. 5*D*). HeLa cells transfected with TrkA present a $LogEC_{50}$ of −9.219 ± 0.087 (an EC_{50} = 6.03 × 10^{-10} M). In cells coexpressing TrkA and p75, an $LogEC_{50}$ of −9.524 ± 0.176 (an EC_{50} = 2.99 × 10^{-10} M) was found, showing a small but significant effect of p75 on the activation of TrkA by NGF. The parallel curve suggested an agonist effect of p75 and NGF on the activation of TrkA. To analyze the effect of p75-TMD, we used a construct of p75 with its TMD swapped with the one from the TNFR, mutant p75-TNFR. A decrease in the NGF sensitivity was observed in comparison to p75-wt ($LogEC_{50}$ = −8.56 ± 0.54; EC_{50} = 2.7 × 10^{-9} M), indicating that the effect of p75-wt is lost in the p75-TNFR construct. As the protein heterodimer interface contains the motif $A_{261}A_{262}xxxG_{266}xxA_{269}$, we made a construct with a triple mutation A262,G266,A269 to Ile (p75–AGA mutation). The rationale behind this is that the introduction of a hydrophobic bulky residue, Ile, would impair the proper interaction with the TrkA-TMD. Fitting of the values obtained from the lysates transfected with TrkA and p75–AGA showed a $LogEC_{50}$ of −8.776 ± 0.037, which corresponds to an EC_{50} = 1.7 × 10^{-9} M (Fig. 5*D*), that accounts for more than one order of magnitude higher than in the presence of p75-wt supporting that this interface plays a key role in TrkA activity modulation by p75.

p75 needs a specific interface in the TMD to interact to TrkA

The finding that the activation of TrkA in the presence of the p75–AGA mutant is lower than in the absence of p75

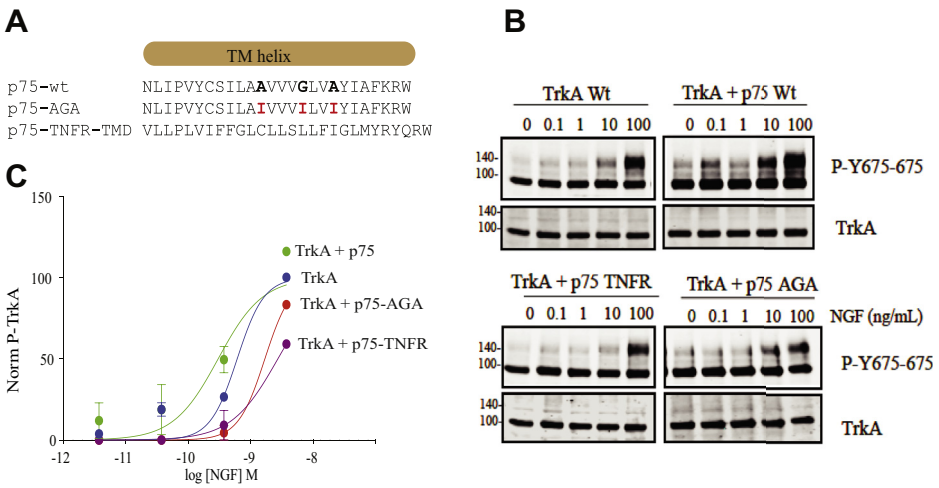

Figure 5. TrkA activation is modulated by p75-TMD. *A*, protein sequences of the different mutant constructs of p75-TMD. The residue mutated is shown in *bold*. *B*, western blots of lysates from HeLa cells transfected with the indicated constructs and stimulated with increasing concentrations of NGF. Membranes were probed using a TrkA-P-Tyr675 specific antibody. *C*, normalized activation of TrkA using increasing concentrations of NGF in the absence or the presence of p75 mutant constructs indicated. The bars represent the standard error of at least three independent experiments. *p* Values are reported in the article. NGF, nerve growth factor; TMD, transmembrane domain; TrkA, tyrosine potein kinase receptor A.

suggested an antagonist or inhibitor behavior for this mutant. To further study the effect of this mutation on the heterodimer complex, we introduced the triple mutation AGA/III into the p75-TMD and performed a CG-MD followed by FA-MD simulation similar to the p75-TMD-wt constructs shown previously (Fig. S3). MD analysis showed that although p75-TMD-AGA mutant still interacts and binds to the TrkA-TMD with similar kinetics as the p75-TMD-wt, the heterodimer arrangement is changed significantly. It has been previously shown that TrkA-TMD contains two homodimer interfaces; an active dimer formed upon NGF binding and an inactive dimer formed in the absence of NGF. The 12 independent simulations of p75-TMD-wt showed a restricted binding interface localized close to the inactive homodimer interface, leaving the active homodimer interface of TrkA free and accessible (Fig. 6*A*). However, after 12 independent simulations, the endpoint of p75-TMD-AGA is almost equally distributed in all the possible TrkA-TMD interfaces (Fig. 6*B*), where the active homodimer interface is hidden by p75-TMD. This result indicates that p75-TMD-AGA could impair TrkA active homodimerization and may explain the weaker activation of TrkA in the presence of p75-TMD-AGA.

p75–AGA/III reduces NGF-induced differentiation of PC12 cells

To further support our finding that p75 needs a specific heterodimer interface to fully activate TrkA, we overexpressed p75-wt and p75–AGA/III in PC12 cells that endogenously express TrkA and quantified the neurite length upon stimulation with NGF. As shown in Figure 6*C*, the PC12 cells transfected with p75–AGA/III had shorter neurite lengths at 24 h than cells transfected with p75-wt (16.02 μm ± 0.98, n = 181 *versus* 22.63 μm ± 1.69, n = 89) and similar length as PC12 cells transfected with the empty vector (14.09 μm ± 1.25, n = 92) (control in Fig. 6*C*). These experiments suggest a reduction in the activation of TrkA by NGF of p75–AGA/III in comparison to p75-wt.

Discussion

The present study provides, to the best of our knowledge, the first structural evidence of a direct interaction between p75 and TrkA. While data from *in vitro* and *in vivo* experiments have suggested the existence of a complex formed by p75 and TrkA (41–43), repeated attempts to observe the direct interaction between both receptors using different biochemical and structural approaches have been unsuccessful. Experimental evidence of the existence of a TrkA–p75 complex were based on coimmunoprecipitation studies (17, 21, 44) and by biophysical methods such as copatching (45) and fluorescence recovery after photobleaching (46). In addition, a handful of studies have suggested that the TMDs and ICDs of p75 could be responsible for its interaction with TrkA (21, 34, 47, 48).

Here, we demonstrated that the complex formed by p75 and TrkA is mediated by the TMDs, supporting the findings by previous reports (21, 34). The results of our NMR titration experiments point to a relatively weak affinity constant, similar to that calculated for p75 noncovalent dimerization. This is around ten times weaker than the affinity constant calculated for glycophorin-A homodimerization and explains why these complexes have been difficult to detect by coimmunoprecipitation in the presence of detergents (*i.e.*, glycophorin A TMD dimers are resistant to SDS-PAGE). Heterocrosslinking

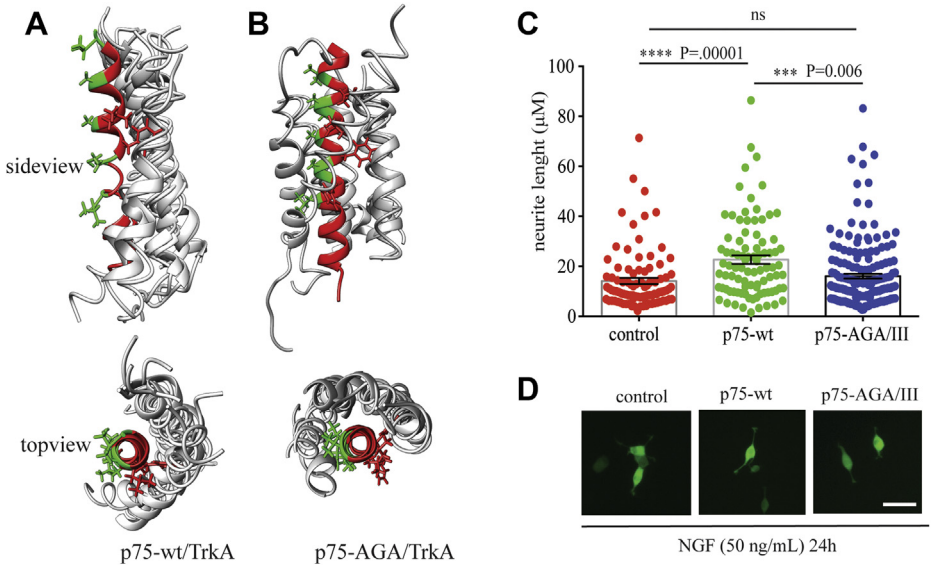

Figure 6. Effect of the mutation of the p75 heterodimer interface. *A* and *B*, result of 12 simulations by CG-MD of p75-TMD-AGA mutant (*A*) or p75-TMD-wt (*B*) and TrkA-TMD in POPC model membranes. The position of the p75-TMD helix (*gray*) respect to the TrkA-TMD (*red*) after each simulation is shown. In *green* and *red* are shown the residues that belong to the active and inactive homodimer interface of TrkA described in the study by Franco *et al.* *C*, quantification of the neurite length (micrometer) of PC12 cells electroporated with the indicated constructs and GFP at 24 h of addition of NGF (50 ng/ml). The bars represent the standard error of at least three independent electroporation experiments. Statistical analysis was performed with one-way ANOVA, and the *p* values are reported above each bar. *D*, representative fluorescence microscopy of PC12 cells electroporated with the indicated constructs stimulated with NGF (50 ng/ml) for 24 h after electroporation. The bar represents 50 μm. CG, coarse-grained; MD, molecular dynamics; NGF, nerve growth factor; POPC, palmitoyl-2-oleoyl-sn-glycero-3-phosphocholine; TMD, transmembrane domain.

experiments similarly failed to detect p75–TrkA complexes, although probably for different reasons, as crosslinking requires the specific residues (*i.e.*, Lys) to be close to each other and oriented in a specific manner, not always possible even in a heterocomplex. Our results are in agreement with those of fluorescence recovery after photobleaching experiments, which show that p75 is fully mobile at the cell membrane but becomes restricted in mobility upon TrkA coexpression (46), and with biochemical evidence suggesting that the TMD of p75 is necessary for the formation of high-affinity NGF-binding sites (34). Although the TMD interaction is weak, *in vivo*, the levels of p75 and Trk normally exist at a ratio of approximately 10:1 (49, 50) favoring their heterointeractions over TrkA homointeractions.

Recently, it has been shown that TrkA has two homodimer interfaces in the TMD; one active and one inactive (36). The active interface corresponds to the TrkA bound to its ligand NGF. And the inactive dimer interface corresponds to the preformed dimer of TrkA in the absence of NGF. The observed binding of p75-TMD to TrkA takes place mainly through an interface that is opposite to the active interface and partially covering part of the inactive dimer interface, suggesting that binding of p75 to TrkA may favor the formation or stabilization of TrkA active homodimers. In addition, stabilization of a preformed dimer would be compatible to an increase in the affinity of TrkA for NGF in the presence of p75 (18), suggesting that the heterodimer p75–TrkA described here forms the basic unit of the NGF high-affinity sites. The finding that mutations in the p75 protein interface, as shown here with the p75–AGA mutant, impact the TrkA activation and supports the requirement of specific TMD interactions in the NT receptors. As it has been shown recently, NGF binding can induce the rotation of the TrkA TM dimer form the inactive to the active interface (36, 51). This conformational change is supported by our FRET analysis, which reveals that NGF binding alters the TrkA–p75 heterocomplex that we observed in the absence of ligand. There are some possible explanations for this result, which are both illustrated in Figure 1*H*. The first option is that NGF binding could cause the dissociation of the TrkA–p75 heterocomplex, stabilizing the respective homodimers instead. Another explanation is that NGF binding induces a conformational change of the TrkA–p75 heterocomplex that alters the positioning of the fluorescent proteins, increasing their separation and thus decreasing the FRET signal. While these data cannot distinguish between these two possible effects, the FRET data clearly demonstrate that TrkA and p75 interact directly in the absence of ligand and that NGF binding alters the heterocomplex.

Our MD analysis of p75–AGA–TrkA interactions showed that the inactive dimer interface is accessible suggesting that p75–AGA interaction may displace the equilibrium toward the inactive homodimer of TrkA in the absence of NGF. This would affect the activation of TrkA and lead to lower cell differentiation capabilities of PC12 cells overexpressing the p75–AGA mutant. Alternatively, the binding of the p75–AGA mutant may affect the conformational change induced by NGF binding resulting in a less activation of TrkA.

Altogether, we show that a specific transmembrane interaction is required for the positive role of p75 in TrkA activation by NGF. In conclusion, we provide a new structural insight on the highly dynamic p75–TrkA heterocomplex, paving the way to new investigations about the biological relevance of such interactions.

Experimental procedures

p75-TM and TrkA-TM constructs for cell-free expression

The gene encoding transmembrane and juxtamembrane residues 245 to 284 (MT245RGTTDNLIPVYCSILAAVVV GLVAYIAFKRWNSSKQNKQ284) of human p75 receptor (p75-TM-wt) was amplified by PCR from six chemically synthesized oligonucleotides (Evrogen) partially overlapped along its sequence. The C257A point mutant form of p75TM (p75-TM-C257A) was obtained by site-directed mutagenesis by PCR. The PCR products were cloned into a pGEMEX-1 vector by three-component ligation using the NdeI, AatII, and BamHI restriction sites. Expression constructs for human TrkA-TM (MK410KDETPFGVSVAVGLAVFACLFLSTLLLVLNKAGRR NK447) were similarly prepared by PCR.

FSI–FRET experiments

HEK 293T cells used in the FRET experiments were purchased from American Type Culture Collection (CRL-3216). The cells were cultured at 37 °C and 5% CO_2 in Dulbecco's modified Eagle's medium (DMEM; Thermo Scientific; 31600-034) containing 3.5 g/l D-glucose, 1.5 g/l sodium bicarbonate, and 10% fetal bovine serum (FBS; Sigma–Aldrich; F4135). HEK 293T cells were seeded in 35-mm glass bottom collagen-coated petri dishes (MatTek Corporation) at a density of 2×10^5 cells/dish and cultured for 24 h. The cells were cotransfected with pcDNA constructs encoding for TrkA tagged with mTurq (the donor) and p75 tagged with eYFP (the acceptor). The TrkA-mTurq plasmid was generated as described (32, 52). The p75-eYFP construct was cloned by overlapping PCR into the same pcDNA vector. The LAT and ECTM FGFR3 plasmids used for control experiments were generated as described previously (53, 54). Transfection was performed with Lipofectamine 3000 (Invitrogen; L3000008) using 1 to 4 μg of total DNA at a TrkA:p75 ratio of 2:1 or 1:1. In addition, cells singly transfected with either TrkA-mTurq or p75-eYFP were used for calibration as described (32). After 12 h following transfection, the cells were washed twice with starvation media (serum-free and phenol red–free media) and serum starved in starvation media for 12 h overnight. Prior to imaging, the starvation media were replaced with hypo-osmotic media (10% starvation media, 90% deionized water, and 25 mM Hepes) to "unwrinkle" the highly ruffled cell membrane under reversible conditions as described (55). Cells were incubated for 10 min and then imaged under these conditions for approximately 1 h. In some experiments, soluble human beta nerve growth factor (Cell Signaling Technology; 5221SC) was diluted to a final concentration of 100 ng/μl with the hypo-osmotic media before adding to the cells.

Cell images were obtained following published protocols (32) with a spectrally resolved two-photon microscope set up using a Zeiss Inverted Axio Observer and the OptiMis True Line Spectral Imaging system (Aurora Spectral Technologies) with line-scanning capabilities (56, 57). Fluorophores were excited with a mode-locked laser (MaiTai, Spectra-Physics) that generates femtosecond pulses between wavelengths 690 and 1040 nm. For each cell, two images were collected: the first at 840 nm to excite the donor and the second at 960 nm to primarily excite the acceptor. Solutions of purified soluble fluorescent proteins (mTurq and eYFP) were produced at known concentrations following a published protocol (58) and imaged at each of these excitation wavelengths. A linear fit generated from the pixel-level intensities of the solution standards was used to calibrate the effective three-dimensional protein concentration, which can be converted into two-dimensional membrane protein concentrations in the cell membrane as described (32). Small micron-sized regions of the cell membrane were selected, and the FRET efficiency, concentration of TrkA-mTurq, and concentration of p75-eYFP present in the cell membrane were quantified using the FSI–FRET software (32).

Cell-free gene expression

Bacterial S30 cell-free extract was prepared from 10 l of cell culture of the *Escherichia coli* Rosetta(DE3)pLysS strain, using a previously described protocol (59–61). Preparative-scale reactions (2–3 ml of reaction mixture) were carried out in 50-ml tubes.

Titration of TrkA and p75 TMDs by NMR

All TrkA–p75 titration 15N-transverse relaxation optimized spectroscopy experiments were carried out at LPR 80, pH 5.9, temperature 318 K with 20 mM sodium phosphate buffer. Two independent sets of experiments were conducted: (1) unlabeled p75-TM-C257A was incrementally added to 0.5 mM sample of 15N-labeled TrkA-TM and (2) unlabeled TrkA-TM was incrementally added to the 0.4 mM sample of 15N-labeled p75-C257A-TM sample to observe p75–TrkA interactions. Intensities of corresponding peaks were measured at each point, population of the p75–p75 dimer, TrkA–TrkA dimer, and TrkA–p75 complex were calculated and plotted against TrkA–p75 molar ratio.

Cross-correlated relaxation of amide groups was measured as described (62) using two transverse relaxation optimized spectroscopy-based experiments with 10.8 ms relaxation delay, recorded in an interleaved mode. Monomer, dimer, and heterodimer crosspeaks of I259, V263, G266, A269, and Y270 of p75-TM-C257A were taken for the analysis, because only these five residues provide the separate and well-resolved signals of the heterodimer (Fig. S1). Cross-correlated relaxation rates were averaged, converted to the rotational diffusion correlation times as described (62) and then to the hydrodynamic radii of the equivalent sphere using the Stokes–Einstein relationship for the rotational diffusion.

Modulation of TrkA activity by p75

HeLa cells were transfected with 1 μg of TrkA and 1 μg of p75 or p75-TNFR using PEI (ratio 10:1). About 24 h after transfection, cells were lifted and split in identical numbers to a 6-well plate. About 48 h after transfection, cells were starved for 2 h with DMEM without serum and stimulated with different concentrations of NGF (from 0 to 100 ng/ml) for 15 min. Cells were washed with PBS and lysed with TNE buffer (Tris–HCl at pH 7.5, 150 mM NaCl, and 1 mM EDTA) on ice for 15 min. Lysates were clarified by centrifugation, and the cell supernatants quantified and analyzed by SDS-PAGE Western immunoblots. Phosphotyrosine-specific antibodies (anti P-Tyr674/675 from Cell Signaling Technology; 1:3000 dilution) and anti-p75 intracellular antibody (Promega) were used. To quantify the effect of p75 on TrkA, we consider an allosteric interaction between p75 and TrkA and fit to a dose–response curve. The protein band corresponding to the phosphotyrosine signal was quantified, and the ratio to the total TrkA was calculated. This is the response to Figure 4. We plot the log of the concentration of NGF *versus* the response, and the curve was fit to a log(agonist) *versus* response (three parameters) equation using the GraphPad software (GraphPad Software, Inc). The equation is Y = bottom + (top–bottom)/(1+10^((LogEC$_{50}$-X))), and the EC$_{50}$ is the concentration of agonist, in this case NGF, that gives a response halfway between bottom and top. At least three independent experiments were quantified.

CG molecular simulation methods

One monomer from the TrkA-TMD dimer structure (Protein Data Bank: 2n90) and one monomer from the p75-TMD dimer structure (Protein Data Bank: 2mic) were converted to a CG model using the script martinize.py from the martini Web page (www.cgmartini.nl) and the tools from GROMACS, version 5.0.5 (www.gromacs.org). In CG models, four heavy atoms are grouped together in one CG bead. Each residue has one backbone bead and zero to four side-chain beads depending on the residue type (63). For all helix dimerization simulations, two α-helices were inserted into a preformed POPC bilayer (containing 260 lipids) such that they were separated by an interhelix distance (dHH) ≈ 55 Å (Fig. 6). Each system was solvated with 2975 CG water particles and 0.15 M NaCl counter ions. The energy of the system was minimized and followed by 12 MD simulations of 5 μs each simulation in a total time of 60 μs. CG simulations were performed using GROMACS, version 5.0.5 (www.gromacs.org) (64). All simulations were performed at constant temperature, pressure, and number of particles. The temperatures of the protein, lipid, and solvent were each coupled separately using the Berendsen algorithm at 305 K, with 774 at a coupling constant of τT = 1 ps. The system pressure was semi-isotropically using the Parrinello–Rahman algorithm at 1 bar with a coupling constant of τP = 12 ps and a compressibility of 3 Å ~ 10^{-4} bar^{-1}. The time step for integration was 20 fs. Coordinates were saved for subsequent analysis every 200 ps.

TrkA and p75 complex formation

Atomic MD

GROMACS, version 5.0.5 was also used for all FA MD simulations. CG models were converted to FA using the CHARMM-GUI portal (www.charmm-gui.org). FA was calculated using the CHARMM36m force field. The van der Waals interactions were smoothly switched off at 10 to 12 Å by a force-switching function. Long-range electrostatic interactions were calculated using the particle mesh Ewald method. The simulations were performed at a temperature of 303.15 K using a Nose–Hoover thermostat with $\tau T = 1$ ps. A constant pressure of 1 bar was maintained with a Parrinello–Rahman algorithm with a semi-isotropic coupling constant $\tau P = 5.0$ ps and compressibility = 4.5 Å $\sim 10^{-5}$ bar^{-1}. The integration time step was 2 fs. The LINear Constraint Solver (LINCS) method was used to constrain bond lengths. Coordinates were saved every 5 ps for analysis. Analysis of all simulations was performed using the GROMACS suite of programs. VMD (65) and Chimera UCSF (66) were used for visualization and graphics. Membrane equilibration was assessed measuring the area per lipid and the membrane thickness using the APLVoro application (67). The electron density profiles were calculated using the *gmx density* tool in GROMACS. A representation of the electron density of the porous organic cage model membrane with TrkA and p75 TMDs is shown in Fig. S2.

Cell culture and transfection

HeLa cells, which do not endogenously express neither TrkA nor p75, were cultured in DMEM (Fisher) supplemented with 10% FBS (Fisher) at 37 °C in a humidified atmosphere with 5% CO_2. PC12 and PC12nnr5 cells were cultured in DMEM with 10% FBS and 5% horse serum. Transfection in HeLa cells was performed using PEI (Sigma) at 1 to 2 μg/μl. We found that by using PEI as the transfection reagent in HeLa cells, the transfection is suboptimal (10–15% of cells transfected) that allow having a small amount of TrkA expressed in the cells. As a comparison using the same PEI–DNA ratio in HEK 293T cells, TrkA is expressed in higher amounts and ligand-independent activation is seen at these quantities of TrkA DNA. About 500 to 1000 ng of DNA per plate was used in TrkA activation experiments. About 24 h after transfection, cells were lifted and replated in 12-well plates with 100,000 cells per well. Using this procedure, the percentage of transfection is identical in all the wells. About 48 h after transfection, the cells were starved with serum-free medium for 2 h and stimulated with NGF (Alomone) at the indicated concentrations and time intervals. Cells were lysed with TNE buffer (Tris–HCl at pH 7.5, 150 mM NaCl, and 1 mM EDTA) supplemented with 1% Triton X-100 (Sigma), protease inhibitors (Roche), 1 mM PMSF (Sigma), 123 mM sodium orthovanadate (Sigma), and 1 mM sodium fluoride 545 (Sigma). The lysates containing p75 were supplemented with iodoacetamide (Sigma) to avoid postlysate dimer disulfide formation. Lysates were kept on ice for 10 min and centrifuged at 13,000 rpm for 15 min on a tabletop centrifuge. The lysates were quantified using a Bradford kit (Pierce) and analyzed by SDS-PAGE or used in immunoprecipitation.

Western blot analysis

Cells were washed in PBS and lysed in cold lysis buffer (50 mM Tris–HCl [pH 7.5], 150 mM NaCl, 1 mM EDTA, 0.1% SDS, 0.1% Triton X-100, 1 mM PMSF, 10 mM NaF, 1 mM Na_2VO_3, 10 mM iodoacetamide, and protease inhibitor cocktail) at 4 °C. Cellular debris was removed by centrifugation at 13,000*g* for 15 min, and protein quantification was performed by Bradford assay. Proteins were resolved in reducing and nonreducing SDS-PAGE gels, and membranes were incubated overnight at 4 °C with the following antibodies: rabbit polyclonal antihuman p75 ICD (1:1000 dilution; Promega); mouse monoclonal anti-HA (1:2000 dilution; Sigma); rabbit polyclonal MBP probe (1:1000 dilution; Santa Cruz); rabbit anti-phosphoTyr674/5 (1:1000 dilution; Cell Signaling); and rabbit anti-TrkA (1:1000 dilution; Millipore). Following incubation with the appropriate secondary antibody, membranes were imaged using enhanced chemiluminescence and autoradiography.

Electroporation of PC12 and differentiation experiments

The electroporation of the different plasmids was carried out with the Multiporator (Eppendorf). PC12 cells were grown with DMEM supplemented with 10% FBS and 5% horse serum and antibiotics (gentamycin and penicillin). For electroporation, cells were grown to 70 to 80% confluence on a 10-cm plate and washed with PBS. They were then raised with 3 ml of DMEM and centrifuged for 2.5 min at 500 rpm. The pellet obtained was resuspended in 3 ml of the hypo-osmolar electroporation buffer (KCl 25 mM, KH_2PO_4 0.3 mM, K_2HPO_4 0.85 mH, and pH 7.2), and a viable counting with trypan blue was carried out. 1×10^5 cells, and a concentration of 5 μg/ml of the plasmid of interest (control, wt, or mutant) and a concentration of 5 μg/ml of the plasmid with GFP were transferred to an electroporation cuvette (2 mm wide and 400 μl in volume [Eppendorf]). After optimizing the transfection parameters, it was determined that the best results were obtained with a pulse of 100 μs at 200 V; therefore, the electroporation was carried out under these conditions. Finally, the cells were seeded on a 6-well plate with 2 ml of DMEM supplemented with 5% horse serum (Gibco). At 24 h after transfection, the cells were treated with NGF (50 ng/ml) in order to induce the differentiation of neurites as a function of the plasmid. The length of each neurite was quantified from fluorescence microscopy images using the ImageJ software (National Institutes of Health). Three independent electroporation experiments were analyzed, and at least 100 neurites per each condition were quantified.

Data availability

All the data are contained within the article. CSs from TrkA-TMD and p75-TMD are deposited in the Biological

Magnetic Resonance Data Bank with accession number 25872 for TrkA-TMD and 19673 for p75-TMD.

Supporting information—This article contains supporting information (37).

Acknowledgments—We thank Dr M. D. Paul for the acquisition of the LAT–FGFR3 control FRET dataset.

Author contributions—M. L. F., K. D. N., T. P. L., S. A. G., A. S.-L., K. S. M., K. H., A. S. A., and M. V. investigation; M. L. F., K. D. N., T. P. L., S. A. G., F. A., K. S. M., A. S. A., and M. V. methodology; K. D. N., S. A. G., K. S. M., and M. V. validation; T. P. L., K. S. M., K. H., and M. V. writing–original draft; K. S. M., A. S. A., and M. V. conceptualization; K. S. M., A. S. A., and M. V. supervision; K. S. M., K. H., A. S. A., and M. V. funding acquisition; K. S. M., K. H., and M. V. writing–review and editing.

Funding and additional information—This study was supported by the Spanish Ministry of Economy and Competitiveness (project BFU2013-42746-P and SAF2017-84096-R), the Generalitat Valenciana Prometeo grant 2018/055 (to M. V.), and the National Institutes of Health GM068619 (to K. H.). NMR studies of TRKA-TM and p75-TM were supported by the Russian Science Foundation (grant no. 19-74-30014 to A. S. A.). The content is solely the responsibility of the authors and does not necessarily represent the official views of the National Institutes of Health.

Conflict of interest—The authors declare that they have no conflicts of interest with the contents of this article.

Abbreviations—The abbreviations used are: CG, coarse-grained; CS, chemical shift; DMEM, Dulbecco's modified Eagle's medium; DPC, dodecylphosphocholine; eYFP, enhanced YFP; FA, full-atom; FBS, fetal bovine serum; FGFR3, fibroblast growth factor receptor 3; FSI, fully quantified spectral imaging; ICD, intracellular domain; LAT, linker for the activation of T-cells; LPR, lipid-to-protein ratio; MD, molecular dynamics; mTurq, mTurquoise; NGF, nerve growth factor; NT, neurotrophin; POPC, 1-palmitoyl-2-oleoyl-sn-glycero-3-phosphocholine; TMD, transmembrane domain; TNFR, tumor necrosis factor receptor; TrkA, tyrosine protein kinase receptor A.

References

1. Bothwell, M. (2014) NGF, BDNF, NT3, and NT4. *Handb. Exp. Pharmacol.* **220**, 3–15
2. Ceni, C., Unsain, N., Zeinieh, M. P., and Barker, P. A. (2014) Neurotrophins in the regulation of cellular survival and death. *Handb. Exp. Pharmacol.* **220**, 193–221
3. Chao, M. V. (2003) Neurotrophins and their receptors: A convergence point for many signalling pathways. *Nat. Rev. Neurosci.* **4**, 299–309
4. Hempstead, B. L. (2014) Deciphering proneurotrophin actions. *Handb. Exp. Pharmacol.* **220**, 17–32
5. Lu, B., Nagappan, G., and Lu, Y. (2014) BDNF and synaptic plasticity, cognitive function, and dysfunction. *Handb. Exp. Pharmacol.* **220**, 223–250
6. Friedman, W. J., and Greene, L. A. (1999) Neurotrophin signaling via Trks and p75. *Exp. Cell Res.* **253**, 131–142
7. Huang, E. J., and Reichardt, L. F. (2003) Trk receptors: Roles in neuronal signal transduction. *Annu. Rev. Biochem.* **72**, 609–642
8. Deinhardt, K., and Chao, M. V. (2014) Trk receptors. *Handb. Exp. Pharmacol.* **220**, 103–119
9. Reichardt, L. F. (2006) Neurotrophin-regulated signalling pathways. *Philos. Trans. R. Soc. Lond. B Biol. Sci.* **361**, 1545–1564
10. Kraemer, B. R., Yoon, S. O., and Carter, B. D. (2014) The biological functions and signaling mechanisms of the p75 neurotrophin receptor. *Handb. Exp. Pharmacol.* **220**, 121–164
11. Nykjaer, A., Lee, R., Teng, K. K., Jansen, P., Madsen, P., Nielsen, M. S., Jacobsen, C., Kliemannel, M., Schwarz, E., Willnow, T. E., Hempstead, B. L., and Petersen, C. M. (2004) Sortilin is essential for proNGF-induced neuronal cell death. *Nature* **427**, 843–848
12. Mi, S., Lee, X., Shao, Z., Thill, G., Ji, B., Relton, J., Levesque, M., Allaire, N., Perrin, S., Sands, B., Crowell, T., Cate, R. L., McCoy, J. M., and Pepinsky, R. B. (2004) LINGO-1 is a component of the Nogo-66 receptor/p75 signaling complex. *Nat. Neurosci.* **7**, 221–228
13. Wang, K. C., Kim, J. A., Sivasankaran, R., Segal, R., and He, Z. (2002) P75 interacts with the Nogo receptor as a co-receptor for Nogo, MAG and OMgp. *Nature* **420**, 74–78
14. Hempstead, B. L., Martin-Zanca, D., Kaplan, D. R., Parada, L. F., and Chao, M. V. (1991) High-affinity NGF binding requires coexpression of the trk proto-oncogene and the low-affinity NGF receptor. *Nature* **350**, 678–683
15. Kanning, K. C., Hudson, M., Amieux, P. S., Wiley, J. C., Bothwell, M., and Schecterson, L. C. (2003) Proteolytic processing of the p75 neurotrophin receptor and two homologs generates C-terminal fragments with signaling capability. *J. Neurosci.* **23**, 5425–5436
16. Skeldal, S., Sykes, A. M., Glerup, S., Matusica, D., Palstra, N., Autio, H., Boskovic, Z., Madsen, P., Castrén, E., Nykjaer, A., and Coulson, E. J. (2012) Mapping of the interaction site between sortilin and the p75 neurotrophin receptor reveals a regulatory role for the sortilin intracellular domain in p75 neurotrophin receptor shedding and apoptosis. *J. Biol. Chem.* **287**, 43798–43809
17. Jung, K.-M., Tan, S., Landman, N., Petrova, K., Murray, S., Lewis, R., Kim, P. K., Kim, D. S., Ryu, S. H., Chao, M. V., and Kim, T.-W. (2003) Regulated intramembrane proteolysis of the p75 neurotrophin receptor modulates its association with the TrkA receptor. *J. Biol. Chem.* **278**, 42161–42169
18. Bothwell, M. (1995) Functional interactions of neurotrophins and neurotrophin receptors. *Annu. Rev. Neurosci.* **18**, 223–253
19. Chao, M. V., and Hempstead, B. L. (1995) p75 and Trk: A two-receptor system. *Trends Neurosci.* **18**, 321–326
20. Yano, H., and Chao, M. V. (2000) Neurotrophin receptor structure and interactions. *Pharm. Acta Helv.* **74**, 253–260
21. Bibel, M., Hoppe, E., and Barde, Y. A. (1999) Biochemical and functional interactions between the neurotrophin receptors trk and p75NTR. *EMBO J.* **18**, 616–622
22. Rifkin, J. T., Todd, V. J., Anderson, L. W., and Lefcort, F. (2000) Dynamic expression of neurotrophin receptors during sensory neuron genesis and differentiation. *Dev. Biol.* **227**, 465–480
23. White, F. A., Silos-Santiago, I., Molliver, D. C., Nishimura, M., Phillips, H., Barbacid, M., and Snider, W. D. (1996) Synchronous onset of NGF and TrkA survival dependence in developing dorsal root ganglia. *J. Neurosci.* **16**, 4662–4672
24. Mahadeo, D., Kaplan, L., Chao, M. V., and Hempstead, B. L. (1994) High affinity nerve growth factor binding displays a faster rate of association than p140trk binding. Implications for multi-subunit polypeptide receptors. *J. Biol. Chem.* **269**, 6884–6891
25. Lee, K. F., Davies, A. M., and Jaenisch, R. (1994) p75-deficient embryonic dorsal root sensory and neonatal sympathetic neurons display a decreased sensitivity to NGF. *Development* **120**, 1027–1033
26. Davies, A. M., Lee, K. F., and Jaenisch, R. (1993) p75-deficient trigeminal sensory neurons have an altered response to NGF but not to other neurotrophins. *Neuron* **11**, 565–574
27. Majdan, M., and Miller, F. D. (1999) Neuronal life and death decisions functional antagonism between the Trk and p75 neurotrophin receptors. *Int. J. Dev. Neurosci.* **17**, 153–161
28. Majdan, M., Walsh, G. S., Aloyz, R., and Miller, F. D. (2001) TrkA mediates developmental sympathetic neuron survival *in vivo* by silencing an ongoing p75NTR-mediated death signal. *J. Cell Biol.* **155**, 1275–1285
29. Yoon, S. O., Casaccia-Bonnefil, P., Carter, B., and Chao, M. V. (1998) Competitive signaling between TrkA and p75 nerve growth factor receptors determines cell survival. *J. Neurosci.* **18**, 3273–3281

30. Lee, K. F., Li, E., Huber, L. J., Landis, S. C., Sharpe, A. H., Chao, M. V., and Jaenisch, R. (1992) Targeted mutation of the gene encoding the low affinity NGF receptor p75 leads to deficits in the peripheral sensory nervous system. *Cell* **69**, 737–749
31. Wehrman, T., He, X., Raab, B., Dukipatti, A., Blau, H., and Garcia, K. C. (2007) Structural and mechanistic insights into nerve growth factor interactions with the TrkA and p75 receptors. *Neuron* **53**, 25–38
32. King, C., Stoneman, M., Raicu, V., and Hristova, K. (2016) Fully quantified spectral imaging reveals *in vivo* membrane protein interactions. *Integr. Biol. (Camb.)* **8**, 216–229
33. King, C., Raicu, V., and Hristova, K. (2017) Understanding the FRET signatures of interacting membrane proteins. *J. Biol. Chem.* **292**, 5291–5310
34. Esposito, D., Patel, P., Stephens, R. M., Perez, P., Chao, M. V., Kaplan, D. R., and Hempstead, B. L. (2001) The cytoplasmic and transmembrane domains of the p75 and Trk A receptors regulate high affinity binding to nerve growth factor. *J. Biol. Chem.* **276**, 32687–32695
35. Nadezhdin, K. D., García-Carpio, I., Goncharuk, S. A., Mineev, K. S., Arseniev, A. S., and Vilar, M. (2016) Structural basis of p75 transmembrane domain dimerization. *J. Biol. Chem.* **291**, 12346–12357
36. Franco, M. L., Nadezhdin, K. D., Goncharuk, S. A., Mineev, K. S., Arseniev, A. S., and Vilar, M. (2020) Structural basis of the transmembrane domain dimerization and rotation in the activation mechanism of the TRKA receptor by nerve growth factor. *J. Biol. Chem.* **295**, 275–286
37. Kot, E. F., Wang, Y., Goncharuk, S. A., Zhang, B., Arseniev, A. S., Wang, X., and Mineev, K. S. (2020) Oligomerization analysis as a tool to elucidate the mechanism of EBV latent membrane protein 1 inhibition by pentamidine. *Biochim. Biophys. Acta Biomembr.* **1862**, 183380
38. Lesovoy, D. M., Mineev, K. S., Bragin, P. E., Bocharova, O. V., Bocharov, E. V., and Arseniev, A. S. (2017) NMR relaxation parameters of methyl groups as a tool to map the interfaces of helix-helix interactions in membrane proteins. *J. Biomol. NMR* **69**, 165–179
39. Chavent, M., Chetwynd, A. P., Stansfeld, P. J., and Sansom, M. S. P. (2014) Dimerization of the EphA1 receptor tyrosine kinase transmembrane domain: Insights into the mechanism of receptor activation. *Biochemistry* **53**, 6641–6652
40. Shahane, G., Ding, W., Palaiokostas, M., and Orsi, M. (2019) Physical properties of model biological lipid bilayers: Insights from all-atom molecular dynamics simulations. *J. Mol. Model.* **25**, 76
41. Chang, M.-S., Arevalo, J. C., and Chao, M. V. (2004) Ternary complex with Trk, p75, and an ankyrin-rich membrane spanning protein. *J. Neurosci. Res.* **78**, 186–192
42. Zampieri, N., and Chao, M. V. (2006) Mechanisms of neurotrophin receptor signalling. *Biochem. Soc. Trans.* **34**, 607–611
43. Franco, M. L., García-Carpio, I., Comaposada-Baró, R., Escribano-Saiz, J. J., Chávez-Gutiérrez, L., and Vilar, M. (2021) TrkA-mediated endocytosis of p75-CTF prevents cholinergic neuron death upon γ-secretase inhibition. *Life Sci. Alliance* **4**, e202000844
44. Huber, L. J., and Chao, M. V. (1995) A potential interaction of p75 and trkA NGF receptors revealed by affinity crosslinking and immunoprecipitation. *J. Neurosci. Res.* **40**, 557–563
45. Ross, A. H., Daou, M. C., McKinnon, C. A., Condon, P. J., Lachyankar, M. B., Stephens, R. M., Kaplan, D. R., and Wolf, D. E. (1996) The neurotrophin receptor, gp75, forms a complex with the receptor tyrosine kinase TrkA. *J. Cell Biol.* **132**, 945–953
46. Wolf, D. E., McKinnon, C. A., Daou, M. C., Stephens, R. M., Kaplan, D. R., and Ross, A. H. (1995) Interaction with TrkA immobilizes gp75 in the high affinity nerve growth factor receptor complex. *J. Biol. Chem.* **270**, 2133–2138
47. Iacaruso, M. F., Galli, S., Martí, M., Villalta, J. I., Estrin, D. A., Jares-Erijman, E. A., and Pietrasanta, L. I. (2011) Structural model for p75(NTR)-TrkA intracellular domain interaction: A combined FRET and bioinformatics study. *J. Mol. Biol.* **414**, 681–698
48. Sykes, A. M., Palstra, N., Abankwa, D., Hill, J. M., Skeldal, S., Matusica, D., Venkatraman, P., Hancock, J. F., and Coulson, E. J. (2012) The effects of transmembrane sequence and dimerization on cleavage of the p75 neurotrophin receptor by γ-secretase. *J. Biol. Chem.* **287**, 43810–43824
49. Holtzman, D. M., Kilbridge, J., Li, Y., Cunningham, E. T., Lenn, N. J., Clary, D. O., Reichardt, L. F., and Mobley, W. C. (1995) TrkA expression in the CNS: Evidence for the existence of several novel NGF-responsive CNS neurons. *J. Neurosci.* **15**, 1567–1576
50. Verge, V. M., Merlio, J. P., Grondin, J., Ernfors, P., Persson, H., Riopelle, R. J., Hökfelt, T., and Richardson, P. M. (1992) Colocalization of NGF binding sites, trk mRNA, and low-affinity NGF receptor mRNA in primary sensory neurons: Responses to injury and infusion of NGF. *J. Neurosci.* **12**, 4011–4022
51. Ahmed, F., Paul, M. D., and Hristova, K. (2020) The biophysical basis of receptor tyrosine kinase ligand functional selectivity: Trk-B case study. *Biochem. J.* **477**, 4515–4526
52. Ahmed, F., and Hristova, K. (2018) Dimerization of the Trk receptors in the plasma membrane: Effects of their cognate ligands. *Biochem. J.* **475**, 3669–3685
53. Paul, M. D., Grubb, H. N., and Hristova, K. (2020) Quantifying the strength of heterointeractions among receptor tyrosine kinases from different subfamilies: Implications for cell signaling. *J. Biol. Chem.* **295**, 9917–9933
54. Chen, L., Novicky, L., Merzlyakov, M., Hristov, T., and Hristova, K. (2010) Measuring the energetics of membrane protein dimerization in mammalian membranes. *J. Am. Chem. Soc.* **132**, 3628–3635
55. Sinha, B., Köster, D., Ruez, R., Gonnord, P., Bastiani, M., Abankwa, D., Stan, R. V., Butler-Browne, G., Vedie, B., Johannes, L., Morone, N., Parton, R. G., Raposo, G., Sens, P., Lamaze, C., *et al.* (2011) Cells respond to mechanical stress by rapid disassembly of caveolae. *Cell* **144**, 402–413
56. Raicu, V., Stoneman, M. R., Fung, R., Melnichuk, M., Jansma, D. B., Pisterzi, L. F., Rath, S., Fox, M., Wells, J. W., and Saldin, D. K. (2009) Determination of supramolecular structure and spatial distribution of protein complexes in living cells. *Nat. Photon.* **3**, 107–113
57. Biener, G., Stoneman, M. R., Acbas, G., Holz, J. D., Orlova, M., Komarova, L., Kuchin, S., and Raicu, V. (2013) Development and experimental testing of an optical micro-spectroscopic technique incorporating true line-scan excitation. *Int. J. Mol. Sci.* **15**, 261–276
58. Sarabipour, S., King, C., and Hristova, K. (2014) Uninduced high-yield bacterial expression of fluorescent proteins. *Anal. Biochem.* **449**, 155–157
59. Aoki, M., Matsuda, T., Tomo, Y., Miyata, Y., Inoue, M., Kigawa, T., and Yokoyama, S. (2009) Automated system for high-throughput protein production using the dialysis cell-free method. *Protein Expr. Purif.* **68**, 128–136
60. Kai, L., Roos, C., Haberstock, S., Proverbio, D., Ma, Y., Junge, F., Karbyshev, M., Dötsch, V., and Bernhard, F. (2012) Systems for the cell-free synthesis of proteins. *Methods Mol. Biol.* **800**, 201–225
61. Schwarz, D., Junge, F., Durst, F., Frölich, N., Schneider, B., Reckel, S., Sobhanifar, S., Dötsch, V., and Bernhard, F. (2007) Preparative scale expression of membrane proteins in Escherichia coli-based continuous exchange cell-free systems. *Nat. Protoc.* **2**, 2945–2957
62. Chill, J. H., Louis, J. M., Baber, J. L., and Bax, A. (2006) Measurement of 15N relaxation in the detergent-solubilized tetrameric KcsA potassium channel. *J. Biomol. NMR* **36**, 123–136
63. Monticelli, L., Kandasamy, S. K., Periole, X., Larson, R. G., Tieleman, D. P., and Marrink, S.-J. (2008) The MARTINI coarse-grained force field: Extension to proteins. *J. Chem. Theory Comput.* **4**, 819–8345
64. Van Der Spoel, D., Lindahl, E., Hess, B., Groenhof, G., Mark, A. E., and Berendsen. (2005) GROMACS: fast, flexible, and free. *J. Comput. Chem.* **26**, 1701–1718
65. Humphrey, W., Dalke, A., and Schulten, K. (1996) VMD: visual molecular dynamics. *J. Mol. Graph.* **14**, 33–38
66. Pettersen, E. F., Goddard, T. D., Huang, C. C., Couch, G. S., Greenblatt, D. M., Meng, E. C., and Ferrin, T. E. (2004) UCSF Chimera—a visualization system for exploratory research and analysis. *J. Comput. Chem.* **25**, 1605–1612
67. Lukat, G., Krüger, J., and Sommer, B. (2013) APL@Voro: A Voronoi-based membrane analysis tool for GROMACS trajectories. *J. Chem. Inf. Model.* **53**, 2908–2925